Experimental analysis and modelling of fatigue behaviour of thick woven laminated composites

Pongsak Nimdum[1], Jacques Renard[2]

1. Department of Mechanical and Aerospace Engineering
DMIE Center, King Mongkut's University of Technology North Bangkok
1518 Pibulsongkram Rd., Bangsue, Bangkok 10800, Thailand
Pongsak.n@eng.kmutnb.ac.th

2. Centre des Matériaux P.M.Fourt
Mines-Paris Tech, CNRS UMR 7633
BP87, F-91003 Evry cedex, France

ABSTRACT. *The objective of this work was to analyse the fatigue behaviour and the damage development in unidirectional and angle-ply 2/2 twill weave T800 carbon/epoxy woven fabric composite laminates. Fatigue tensile-tensile tests were performed and internal damage has been observed by using camera and optical microscope during testing. The experimental results show that the damage evolution can be characterized by two or three stages according to the 0° ply and angle-ply laminates respectively. An original fatigue criterion for onset delamination during fatigue loading of angle-ply laminates has been proposed. Validation of fatigue model was made with tensile fatigue tests performed on angle-ply textile laminates with drilled circular hole. Further numerical predictions are in good agreement with experimental results.*

RÉSUMÉ. *L'objectif de cette étude est d'analyser l'ensemble des comportements mécaniques et des mécanismes d'endommagement dans un composite tissé (2x2 twill) T800 carbone/époxy. Des essais en traction-traction de fatigue ont été faits en observant les évolutions des endommagements par caméra optique. Les résultats expérimentaux montrent que l'évolution des endommagements se décompose en deux ou trois étapes selon les orientations des plis (pli unidirectionnel ou pli croisé). Un modèle d'initiation du délaminage en fatigue a été également proposé. La validation de ce modèle a été ensuite étudiée sur une plaque composite trouée soumis à des sollicitations de fatigue en traction-traction. Le calcul numérique montre une bonne corrélation avec ces résultats expérimentaux.*

KEYWORDS: *carbon fibre, thick woven composite, fatigue model, damage mechanism, FEM.*

MOTS-CLÉS : *fibres de carbone, composite épais, modèle de fatigue, mécanismes d'endommagement, calculs par éléments finis*

DOI:10.3166/RCMA.26.87-113

1. Introduction

Composite materials have been widely used in high performance structures especially in automobile, wind turbine blades, marine industries, aircrafts, sports equipment, railway structure, etc. However, the application of unidirectional composites has several drawbacks such as impact resistance and tolerance in presence of a delamination. Therefore, the trend for composites applications is undergoing a transition towards the use of textile composite, also known as "woven fabric composites". These materials present various attractive (Nicoletto et Riva, 2004; Kelkar *et al.*, 2006; Alif *et al.*, 1998) since it provides improved impact resistance, better in out-of-plane mechanical properties and improved damage tolerant in the presence of the delamination due to the non-planar interply structure of woven fabric composites. Nevertheless, the stiffness and strength behaviour of woven fabric composites are dependent on many parameters such as the characteristics of fibers and matrix and weave architecture (Pandita *et al.* 2001) (weave type, packing density of yarns, undulation angle etc.).

Thus, the woven carbon fabric/epoxy composite laminates present all their interest. The purpose of this work is to first present the damage mechanisms and to focus on the correlation between damage accumulation and mechanical property. Then, the finite element method (FEM) is applied for representing the failure mechanism and mechanical damage. Finally, we shall propose a criterion for onset of delamination under cyclic loading extended from static criteria.

2. Experimental procedure

2.1. Material

The composite material of this study was carried out on carbon (T800)/epoxy composite material. The carbon fiber density was 12.81 g/cm^3. The diameter of carbon fiber is equal 7 μm. This study focuses on woven fabrics composites which the interlacing of the fill and warp yarns was formed according to the 2/2 twill weave pattern as show in Figure 1 with 0.65 mm for one ply thickness and the resulting fiber volume fraction V_f = 52.9% . The presence of weave structure induces very specific physical phenomena. Therefore, first we study on woven 0°-ply laminate i.e. each ply of laminate is similar orientation and then we study on woven angle-ply laminates $((0°,\pm20°)_s$, $(0°,\pm20°2)_s$, $(0°,\pm30°)_s$ and $(0°, \pm30°2)_s)$.

In case of woven 0°-ply laminate, twill 2/2 weave has the same number of yarns in both directions such as fill ($\vec{x}_1$) and warp ($\vec{x}_2$) direction to provide balanced bi-directional properties in fabric plane. Figure 2 shows the schema of woven fabrics. The unit cell is a square and composed of 4x4 yarns corresponding to about 9.2x9.2 mm^2. For this study, we perform on a thick composite consisting of several layers, this result that many different patterns were occurred in 0°-ply laminates. In order to simplify in this study, we can classify in three significant cases such in-phase (IP), out-of-phase (OP) and intermediate phase (T90) (Figure 2).

In the case of angle-ply woven laminates, each ply is supposed to be a homogenous material.

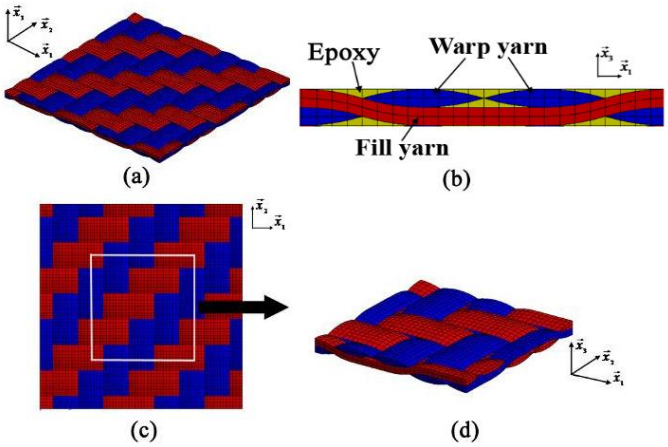

Figure 1. (a) Scheme of the 2x2 twill weave architecture; (b) three elements of woven fabrics; (c) weave architecture – top view and (d) unit cells

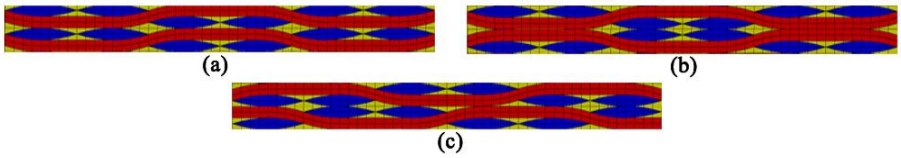

*Figure 2. Different pattern possibilities in woven **0°**-ply laminates: (a) in-phase (IP); (b) out-of-phase (OP) and (c) T90*

2.2. Experimental procedure

Fatigue tension-tension loading was applied on hydraulic testing system (Figure 3a). We chose to perform a load control mode. Axial extensometer is used to measure the longitudinal elongation. The changes in load and longitudinal displacement during fatigue tests are recorded.

It is assumed that the material behaviour is linear to avoid strain rate effects consideration (or frequency effect). Fatigue tension-tension tests was performed with: (i) the difference of maximum applied stress ($\sigma_{\max}$) from which woven 0°-ply laminate will be performed at $0.3\sigma_R$, $0.5\sigma_R$ and $0.7\sigma_R$ while woven angle-ply laminates will be performed at $0.4\sigma_R$, $0.5\sigma_R$ and $0.6\sigma_R$ where σ_R is the ultimate stress ; (ii) the ratio minimum to maximum stress (R), also called the load ratio, in a

cycle was 0.1, (ii) the frequency (f) is 1 Hz, and (iii) all tests are performed at room temperature.

All specimens were cut from plates using the diamond wheel saw and were bonded with glass/epoxy or aluminium tabs onto each specimen end. During fatigue tests, the specimen surface (length 65 mm) is recorded at loading less than the maximum applied stress (Figure 3b) with a digital CCD camera under white light illumination.

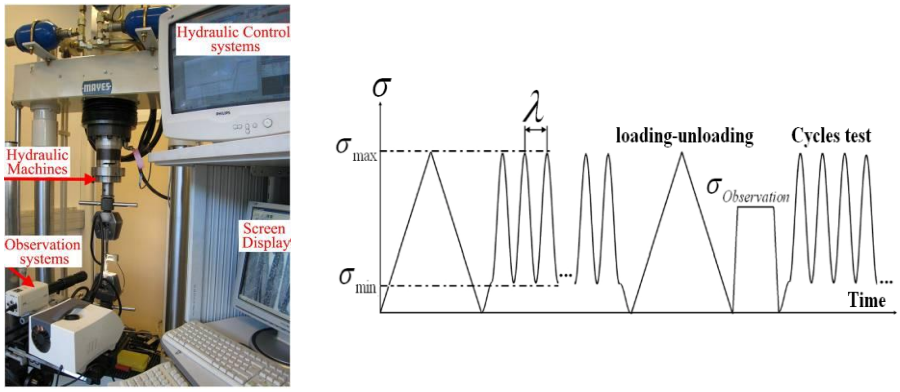

(a) (b)

Figure 3. Experimental setup: (a) hydraulic machine; (b) profile of tensile-tensile fatigue tests

3. Experimental analysis under fatigue loading

3.1. Experimental analysis on 0°-ply laminates

3.1.1. Damage mechanism

Figure 4-6 shows that the main fatigue damage mechanisms are ply-cracking, also called transverse cracking, (see “a” in Figure 4) and the intralaminar delamination (see “b” in Figure 4). Generally, these delaminations are initiated at the edges of the specimen (“a” in Figure 5). However, the observation of surface perpendicular to loading direction using ZEISS optical microscopy, show that intralaminar delamination does not only appear at free edges, but also inside of the specimens where the adjacent fills yarns bundles meet (see “c” in Figure 6). These delaminations increase with the number of cycles (see “b” in Figure 5 and 6). It should be noted that the delaminations propagate following a curved yarn and then interface between neighbouring yarns (warp/warp, warp/fill and fill/fill). This result corresponds with the final failure surface showing that most layers have been separated by intralaminar delaminations developed upon the interface of yarns without crossing them.

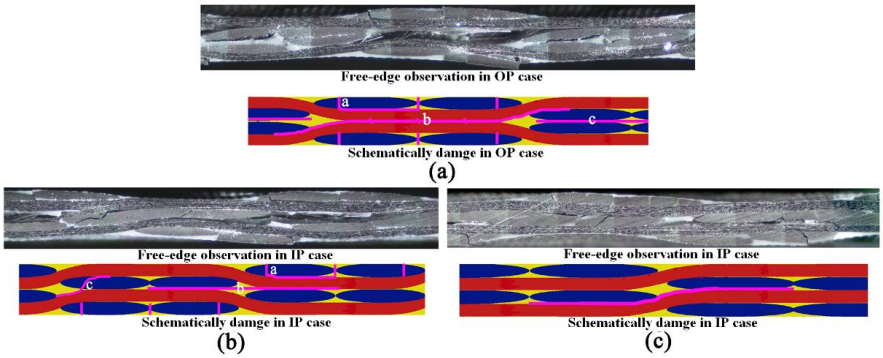

Figure 4. Types of damages during fatigue tests: (a) OP case at $\sigma_{\max} = 0.5\sigma_R$ *; (b) IP case at* $\sigma_{\max} = 0.5\sigma_R$ *and (c) second form of IP case at* $\sigma_{\max} = 0.7\sigma_R$

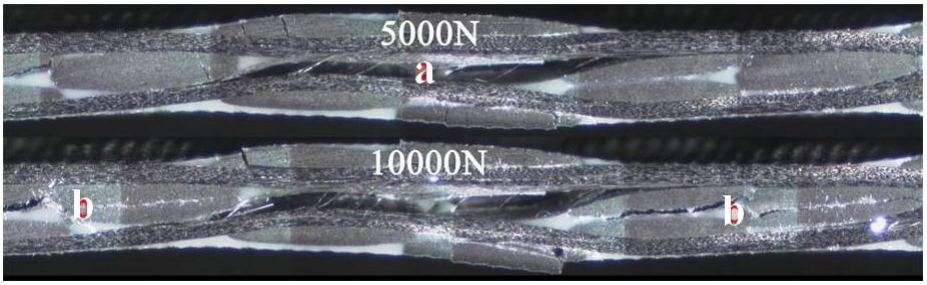

Figure 5. Fatigue damage progression in woven 0°-ply laminates

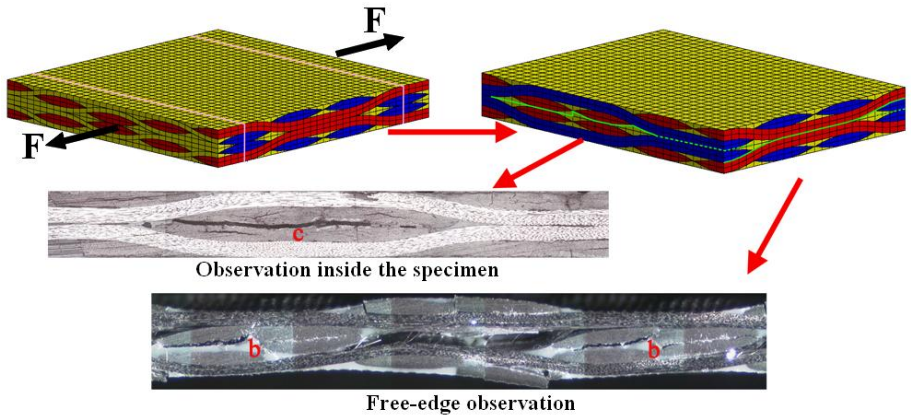

Figure 6. Intralaminar delamination and its progression path on free-edge and inside surface of specimen

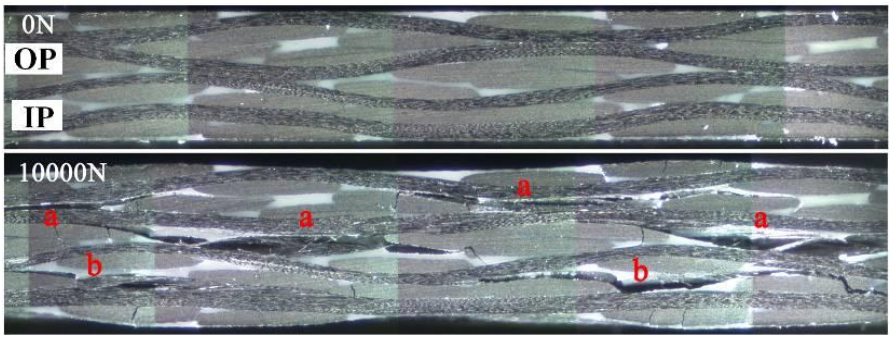

Figure 7. Damage mechanisms in 4 layers. (Fatigue loading at $\sigma_{\max} = 0.7\sigma_R$ *)*

With increasing of number of plies, intralaminar delamination will become more significant and earlier to occur ("a" for OP case and "b" for IP case in Figure 7). On the other hand, transverse cracks are still locally in the surface layer of the specimen and their density remains relatively low.

The observations show that for different maximum applied stress the fatigue damage mechanisms are identical with more rapidly damage evolution when the maximum applied stress increases.

3.1.2. Damage mechanism

If we consider the damage mechanism versus the number of cycles, we found that the damage evolution can be divided into two steps : (i) the initial damage with a threshold number of cycles depend on the pattern of neighbours layers (IP, OP and T90), the maximum applied stress and the number of plies (thickness effect) (ii) then, a rapid increase in density damages and then (iii) finally, saturation of damage density until ending of specimen fracture.

If we now considered the stiffness reduction due to damage evolution as a function of number of cycles, we can identify three stages (Figure 8) (i) a stage I in which a rapid stiffness reduction. This stage corresponds to the delaminations onsets, the multiplication of delaminations until their saturation density and then (ii) a slow decrease stiffness reduction to nearly stabilization. The results of experimental observation show that the regions of intersection of two fills yarn, also called out-of-phase regions, are a preferential position for intralaminar delamination onset.

The fatigue tests in woven 0°-ply laminates with 2, 4, 7 layers for different maximum applied stress show that the effect of the thickness for damage density can be neglected when the number of plies is greater than four (n > 4) (Figure 9). The initiation and progression of damages are more rapidly for thin-plies. Nevertheless, all specimens give close to saturation level of damage density. Reasonably, with increasing maximum applied stress, the saturation density state is still similar but it

is reached more quickly due to the initiation of damages and their progress are more rapidly.

The reduction of rigidity is still related to the damage evolution. In stage II of quasi-stability state of stiffness reduction in which a stiffness reduction of 20-25% occurs whatever the thickness and the maximum applied stress.

It can be seen that the correlation between transverse cracking density and intralaminar delamination density is given. The numerical results, more detail in next section (§4.3), allow to deduce that the onset of intralaminar delamination often leads to the transverse cracking.

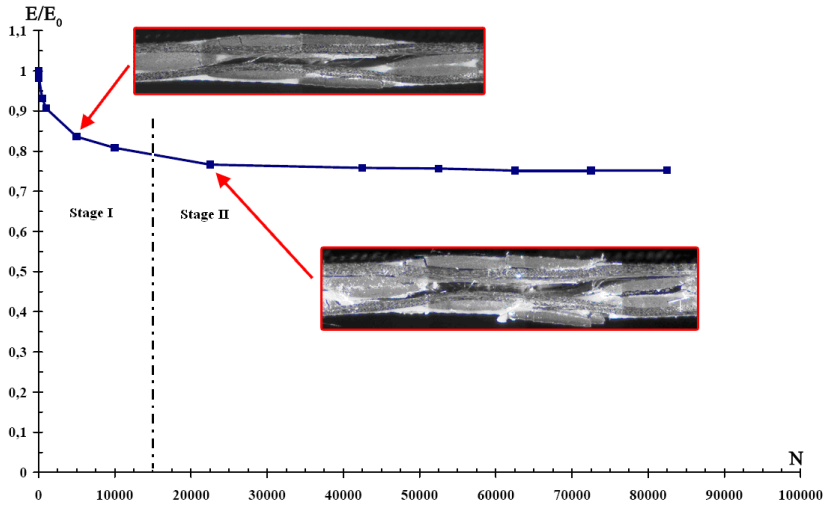

Figure 8. Normalised stiffness property and damage evolution of woven 0°-ply laminates as a function of number of cycles

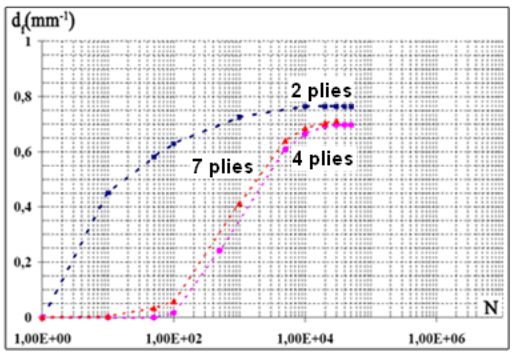

(a)

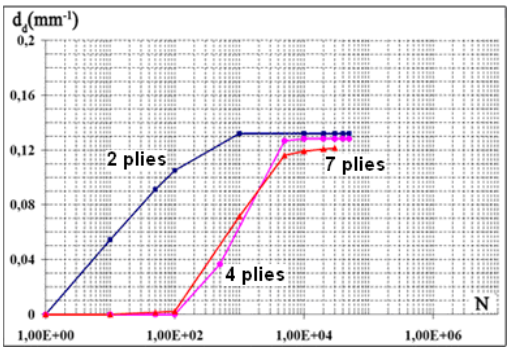

(b)

Figure 9. Normalised stiffness property and damage evolution of woven 0°-ply laminates as a function of number of cycles

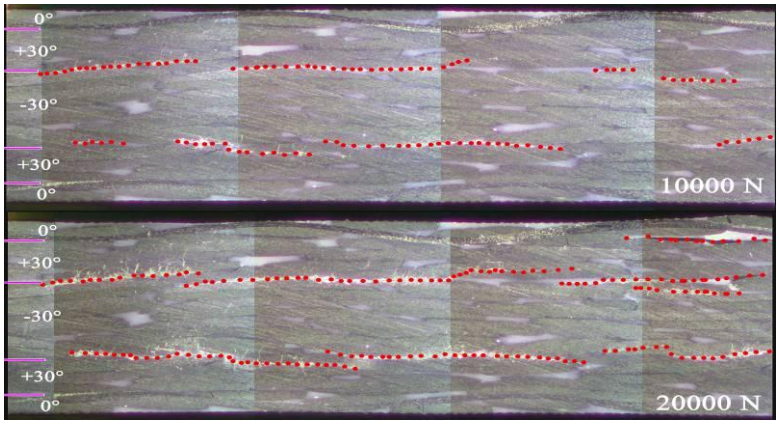

Figure 10. Damage mechanism at $\sigma_{\max} = 0.6\sigma_R$ *versus number of cycles in* $(0°,\pm 30)_s$ *laminate*

3.2. Experimental analysis on angle-ply laminates

3.2.1. Damage mechanism

We now consider the case of the woven angle-ply laminates, $(0°,\pm 20_n)_s$ and $(0°,\pm 30_n)_s$ with $n = 1$ and 2. In generally, due to edge effect lead to free-edge stress singularity at interface of adjacent layers and result in the onset of delamination, also called interlaminar delaminattion. First, the experimental results illustrate the onset delamination at interface $+20°_n/-20°_n$ and $+30°_n/-30°_n$ (Figure 10). These

delaminations are not straight (plan) but bended. They propagate to follow the interface of adjacent yarns and the crimp yarns. These delaminations are considered as shear mode (mode II and III). Then when the number of cycles increases, another mode of delamination appeared at the other interfaces under a mixed-mode of delamination. This result is also a good correlation with static tensile test (Nimdum, 2009). It should be noted that this study is only interest in the delamination onset.

3.2.2. Stiffness degradation

After the interlaminar delamination appeared, we investigate on stiffness degradation and find that the modulus decrease can be divided into three stages (Figure 11): (i) initial region (stage I) with a slightly decrease stiffness reduction of about 2.5%. However, we note that the precision of stiffness reduction measurement related with the observation techniques and then, (ii) an intermediate region (stage II), in which an additional about 10% stiffness reduction occurs in an approximately linear fashion with respect to the number of cycles. Predominant damage mechanisms are the multiplication and development of interlaminar shear delaminations and (iii) the final region (stage III) with a rapid decrease of stiffness (about 40%), and then the stiffness reduction become unstable and lead to the final failure of specimen. Note that increasing of $\sigma_{\max}$ only accelerates to the stiffness degradation (Figure 12).

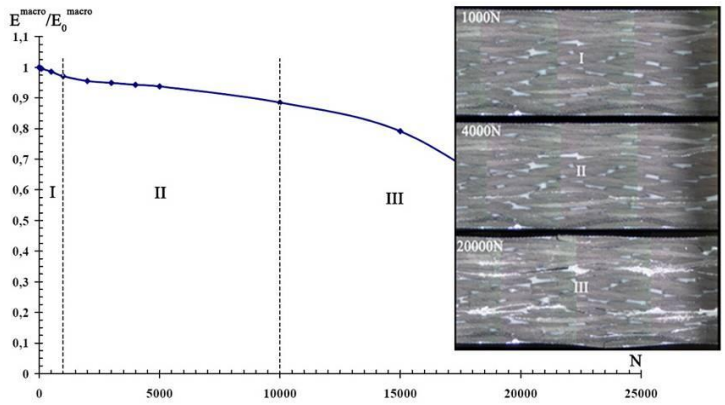

Figure 11. Stiffness degradation as a function of number of cycles

3.2.3. Delamination onset

In order to propose the criterion for prediction the onset of delamination under fatigue loading, we need to determine the relationship among the maximum applied stress ($\sigma_{\max}$), onset of delamination stress under tensile loading test (σ_{onset}) and the number of cycles to delamination onset (N_a). Then, in this study we use four stacking sequences (two different families of laminates each family has two

different thicknesses). By experimental results, the number of cycles to delamination onset as a function of the ratio of σ_{max} to σ_{onset} is illustrated in Figure 13. If the ratio of σ_{max} to σ_{onset} is increase, the early delamination onset is observed. In order that compatible with static test, the ratio of $\sigma_{\max}$ to σ_{onset} is equal to 1, is taken into account. To determine by curve fitting to experimental results (Figure 13), the nonlinear relation between ratio of $\sigma_{\max}$ to σ_{onset} and N_a can then be expressed as $\frac{\sigma_{\max}}{\sigma_R} = \left(K_1\right)^{-(N-1)K2}$ where K_1 and K_2 are two constant parameters, these parameters are independent on i.e. the stacking sequence and number of plies (thickness) but depend on the composite material study.

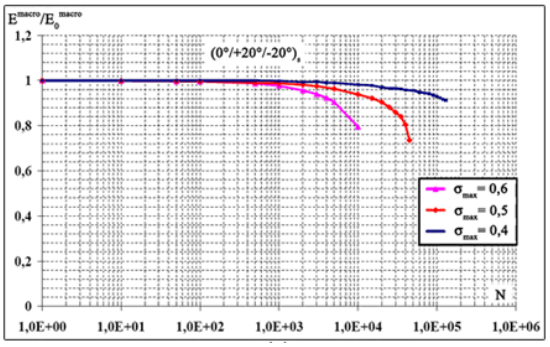

(a)

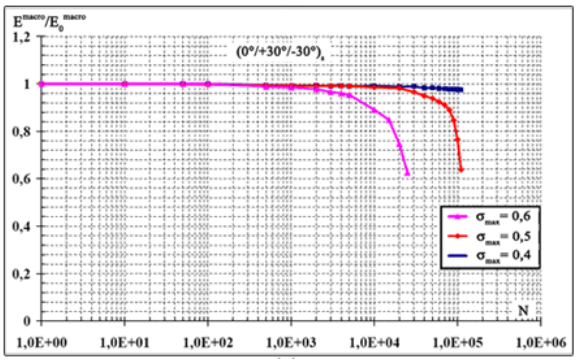

(b)

Figure 12. Stiffness degradation for different $\sigma_{\max}$ *(to compare with* σ_R *) as a function of number of cycles : (a)* $(0°,\pm 20)_s$ *laminate and (b)* $(0°,\pm 30)_s$ *laminate*

This expresion allow to propose the fatigue delamination onset criterion base on quasi-static delamination onset criterion in previous research (Nimdum, 2009).

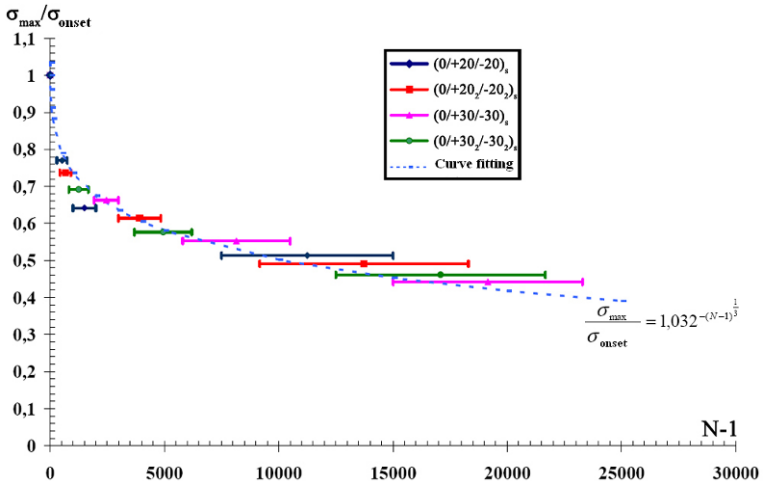

Figure 13. A number of cycles to delamination onset (N_a) in different stacking sequences

4. Experimental procedure

4.1. Configuration

In first part (§4.2), the 3D finite element model of the twill-weave unit cell consists of three-phases (Figure 14): the matrix phase, the warp and fill yarns. This 3D-mesh taken into account the effects of yarns interlacing and orientation of adjacent layers, the geometry of yarns in woven structure is measured directly using optical microscopy observation (Table 1.). Note that due to the complicated structure of weave-fabric, in particularly for crimp region, hence many numbers of finite elements are required.

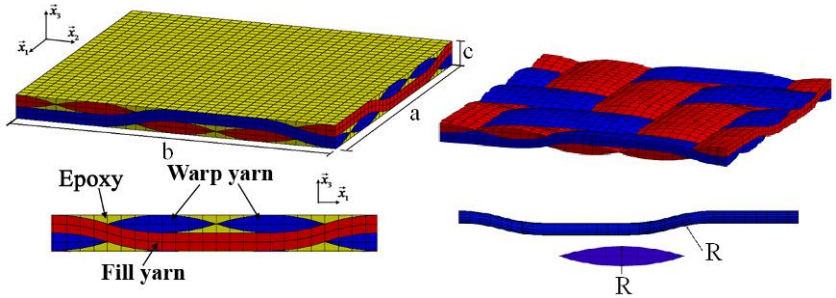

Figure 14. 3D finite element mesh

Table 1. Parameters characterizing the twill-weave geometry (variables are defined in Figure 14. dimensions in mm)

$a=b$	c	R
9.2	0.65	4.15

The mechanical response of a yarn is determined and validated by tensile tests. The yarn (straight region) was assumed transversely isotropic and linear elastic and is given in Table 2, while the property of the epoxy matrix is isotropic elastic with Young's modulus equal to 3.1 GPa and Poisson's ratio equal to 0.39.

However, the second part (§4.3), the 3D finite element model of woven ply (heterogeneous periodic material) are took place by equivalent homogenous ply. Their material behavior determined by homogenization method, as detailed in section 4.2 and 4.3, is show in Table 3. The mesh near the interface corner of free-edge is refined in order to represent the stresses singularity due to the free-edge effect.

Table 2. Mechanical properties of a fill and a warp yarn T800s where 1 refers to the fiber direction; 2 refer to transversal direction of fiber

E_{11} (GPa)	$E_{22} = E_{33}$ (GPa)	G_{23} (GPa)	$G_{12} = G_{13}$ (GPa)	ν_{23}	$\nu_{12} = \nu_{13}$
210.00	9.250	3.7	4.7	0.25	0.33

Table 3. Mechanical properties of an equivalent homogeneous ply of twill-woven fabrics

$E_{11=} E_{22}$ (GPa)	E_{33} (GPa)	$G_{23}=G_{13}$ (GPa)	G_{12} (GPa)	$\nu_{23} = \nu_{13}$	ν_{12}
60.53	7.795	2.685	3.231	0.489	0,0336

4.2. Numerical analysis of damage mechanism

In order to study the effect of curved shape of the reinforcing yarns (weaving structure effect) and adjacent layers, also called ply nesting effect, 3D finite elements model of two layers of twill woven 0°-ply laminate under tensile loading in the fill direction with periodic boundary condition (see in Eq.(1)) are applied. The computational results demonstrate that the weaving structure effect provoke the local bending due to the fill yarn bundles try to straighten. Moreover, the presence of neighboring layers affects to change the local bending direction along the $\vec{x}_3$-axis. The deformed of local symmetrical bending occurred in case of out-of-phase,

otherwise non-symmetrical occurred in case of in-phase and T90 (Figure 15). These results are a good correlation with the experimental observations in previous section.

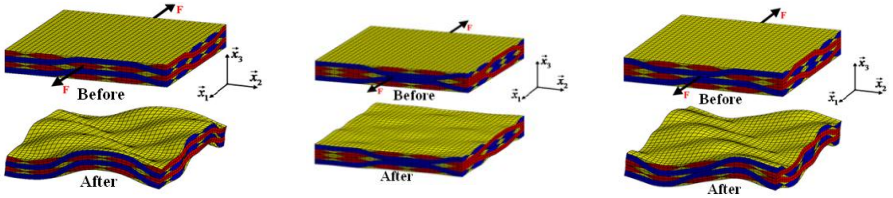

(a) (b) (c)

Figure 15. Deformed mesh of 3D finite element model under unloading and loading: (a) in-phase ; (b) out-of-phase and (c) T90

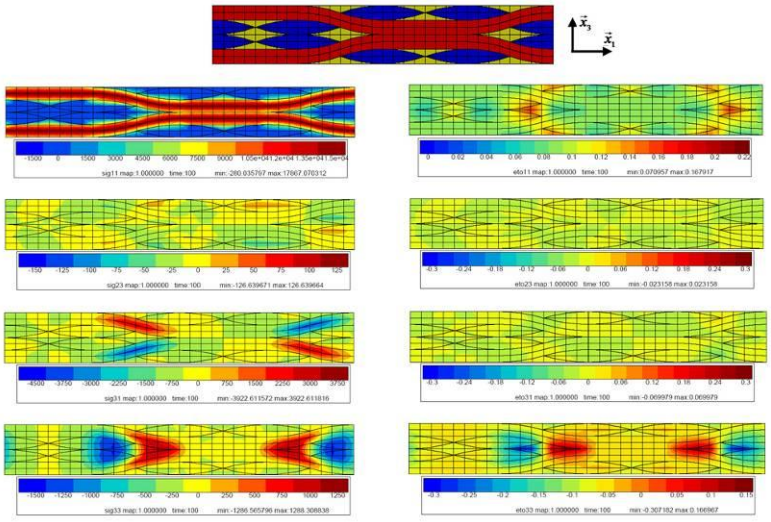

Figure 16. Stress-strain distribution on out-of-phase case

Moreover, the local bending provokes local stress (or strain) concentrations which depend on the ply nesting. The main purpose of this paper is to be interested by investigation of out-of-phase case since the damage mechanisms are earlier to occur and in consequence a rapid decrease of stiffness. Figure 16 shows that high strain ε_{11} occurred in the matrix phase and warp yarns nearly the region of undulation of fill yarns, while, the shear strains ε_{23} and ε_{31} remain relatively homogeneous. On the other hand, non homogeneous strain ε_{33} distribution can be

observed with this maximum strain nearly the region of adjacent fill yarns meet. Besides that increasing of maximum ε_{33} can be induced with increasing of the number of plies. Nevertheless, if woven 0°-ply laminate is more than four-layers ($n > 4$), the thickness effect can be neglected.

4.3. Degradation in 0°-ply laminates

In this section we investigate each damage mechanism, considering at critical or saturation of damage density, affect on the macroscopic mechanical behaviour of the material. Figure 6 was used to describe the geometry of damage to provide the determination of degradation of material due to intralaminar delamination by using 3D finite elements method which enable to simulate the delamination developed in the resin epoxy and at the interface of adjacent yarns (Figure 17). The numerical homogenization procedure is used to determine the global mechanical properties and the periodic boundary conditions in $\vec{x}_1 - \vec{x}_2$ direction were applied. We assume small deformation assumption, therefore the volume variation is quietly small. The microscopic stress $\tilde{\tilde{\Sigma}}_{ij}$ and strain $\tilde{\tilde{E}}_{ij}$ tensors must be the averages of the microscopic corresponding quantities (see in Eq.(1)). In order to simplify the study, we are also assumed that the macroscopic behavior is isotropic in longitudinal and transverse ($\vec{x}_1$ and $\vec{x}_2$, respectively). Besides, this study neglects the friction contact problem when intralaminar delamination appeared.

$$\begin{cases} div\tilde{\sigma} = 0 \\ \tilde{\sigma} = \tilde{\tilde{c}} : \tilde{\varepsilon} \quad \text{on } \Omega \\ \vec{u} = \tilde{\tilde{E}}.\vec{x} + \tilde{v} \quad \text{with } \vec{v} \;\; \vec{x}_1 - \vec{x}_2 \text{ periodic} \\ \vec{u} = \tilde{\tilde{E}}.\vec{x} \;\text{ or }\; \vec{t} = \tilde{\tilde{\Sigma}}.\vec{n} \quad \text{on } \partial\Omega \text{ in } \vec{x}_3 \text{ direction} \\ \tilde{\sigma}.\vec{n} \qquad \vec{x}_1 - \vec{x}_2 \quad \text{anti - periodic on } \partial\Omega \\ \langle\tilde{\sigma}\rangle = \langle\tilde{\Sigma}\rangle \;\text{ or }\; \langle\tilde{\varepsilon}\rangle = \langle\tilde{E}\rangle \end{cases} \tag{1}$$

Figure 18 shows the strains fields in unit cell before and after the intralaminar appeared. The good agreement of two approaches in term of experimental observation and numerical result for damage deformed (Figure 6 and 18). It should to be underline that the redistribution of strains after delamination appeared can be observed (Figure 18b and 18d). The concentration of strain ε_{33} on vicinity of yarns crimping and nearly at interface of two fill yarns and ε_{11} in matrix on vicinity warp yarns inside specimen are vanished, on the other hand, the concentration of ε_{11} on warp surface yarns is increased to allow to understand why the transverse cracks appear immediately on surface warp yarns when the intralamina delamination onset and why their crack is never appeared inside the specimen. Consequently, a good agreement of two damages developed can be observed as an illustration in previous section.

The numerical results provide to determine the elastic coefficients of homogeneous ply equivalent with damaged and non-damaged state to be shown in Table 4. The stiffness reduction, both in tensile and shear modulus by the presence of intralaminar delamination are evident. The absence of constraint on local bending movement due to intralamina delamination onset allow the stretching of fill yarns bundle to become easy, in consequence, the stiffness is considerably reduced. The stiffness reduction of 19.3% is close to experimental results. In order to obviously compare with experimental test, we also simulated the case of transverse cracking. The homogenized response shows that stiffness reduction is slightly and can be neglect. In summary, the intralaminar delamination is predominant on the stiffness reduction in woven 0°-ply laminate.

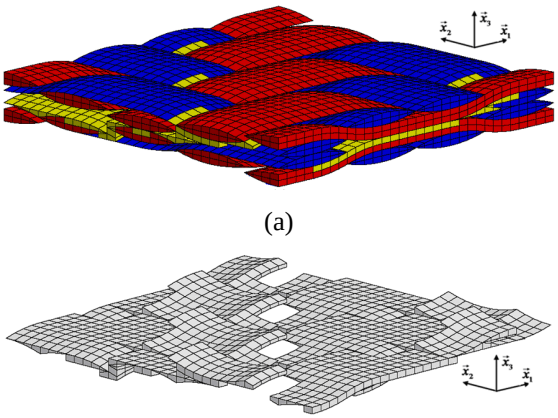

Figure 17. (a) Intralaminar delamination embedded in matrix, fill and warp yarns and (b) mesh configuration of intralaminar delamination

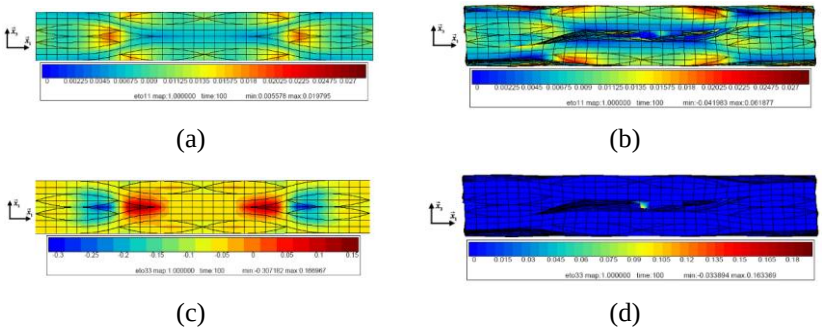

Figure 18. Strains fields: ε_{11} before (a) and after (b) intralaminar delemination onset. ε_{33} before (c) and after (d) intralaminar delemination onset

Table 4. Damages dominants in global stiffness reduction

Macroscopic behavior in unit cell	Non-damage (GPa)	Damage (GPa)	Stiffness reduction (%)
E_{11}	60,53	48.854	19.3
E_{22}	60,53	48.854	19.3
E_{33}	7.795	1.487	80.93
G_{23}	2.685	1.068	60.3
G_{13}	2.685	1.068	60.3
G_{12}	3.231	3.14	2.08

4.4. Prediction of delamination onset under fatigue loading

4.4.1. Introduction

In order to predict the fatigue life and degradation in the composite material, the three categories in previous studies are proposed: (i) empirical approach, also so-called macroscopic failure theories (Fawaz et Ellyin, 1994; Demers, 1998; Bond, 1999) base on static strength criteria modified to account for cyclic loading; (ii) strength or stiffness degradation fatigue criteria (Broutman et Sahu, 1972; Philippidis et Vassilopoulos, 1999) which strength or stiffness are evaluated as a function of number of cyclic loading; (ii) finally actual damage mechanics fatigue theory is base on the modelling of intrinsic defects in the composite material (Talreja, 2003; Thionnet et Renard, 1994; 1997; Caron, 1993).

The first approach is presented in the empirical method and has found widespread use in fatigue analysis although it does not account for plastic deformation during the cyclic loading. This approach is usually plotted in term of *S/N* diagram where *S* is the applied cyclic stress and *N* is the number of cycles.

The second approach of fatigue life is defined by the modified static failure criteria (Hashin et Rotem, 1973) which take on a similar form to the Tsai-Hill criterion and can be written:

$$\sigma_1 = \sigma_1^N$$

$$\left(\frac{\sigma_2}{\sigma_2^N}\right)^2 + \left(\frac{\tau_{12}}{\tau_{12}^N}\right)^2 = 1 \qquad (2)$$

where σ_1, σ_2 and τ_{12} are the in-plane normal, transverse and shear stress, respectively. σ_1^N, σ_2^N and τ_{12}^N are the in-plane normal, transverse and shear fatigue strength as a function given in Eq. (3).

$$\begin{aligned}\sigma_1^N &= \sigma_1^R f_1(\sigma_{\max}, R, N)\\ \sigma_2^N &= \sigma_2^R f_2(\sigma_{\max}, R, N)\\ \tau_{12}^N &= \tau_{12}^R f_{12}(\sigma_{\max}, R, N)\end{aligned} \tag{3}$$

where σ_1^R, σ_2^R and τ_{12}^R represent the in-plane normal, transverse and shear static strength, respectively.

Final approach describes the evolution of material behaviour throughout fatigue cyclic loading using damage progressive model. This approach based on damage mechanics is used to model both the quasi-static and fatigue loading by using the variation of the state function, also called free energy function.

The main aim of this paper is to propose of delamination onset criterion under fatigue loading base on the second approach using the strength degradation, or residual strength. In order to simplify the problem, in this study, stiffness and strength reduction due to intralaminar delamination onset will be neglected and the equivalent homogenous ply is used with in-plan isotropic behaviour (Table 3)

4.4.2. Delamination onset criterion under fatigue loading

The edge effect generally leads to the stress singularities near free-edge interface which occur when we use the finite element analysis method. Consequently the use of local criterion, for delamination onset depends on the mesh size in the free-edge area. In order to avoid the mesh-dependent of finite element approximation, the delamination onset criterion should not only take account of point stress but also their distributions. As a result, many non-local stress criteria have been developed. We can classify them into two categories.

The first category of criteria (Lorriot, 2003; Kim et Soni, 1984; Brewer et Lagace, 1988; Joo, 1992) is based on the average stress, often using an integral method, over an area or a line. In this study non-local stress criteria corresponding to the three anti-plane stresses which are defines as

$$\overline{\sigma}_{ij}(y_0) = \frac{1}{y_0}\int_0^{y_0} \sigma_{ij}(\xi) d\xi \tag{4}$$

where σ_{ij} and $\overline{\sigma}_{ij}$ represent three local anti-plane stresses and average anti-plane stresses at interface, respectively. y_0 is the critical length over which three average stresses are determined.

Then, the second categories of criterions represented the gradient of stress singularities using the weight function which allow to evaluate the weight changes in quantities (Bažant et Pijaudier-Cabot, 1998; Germain *et al.*, 2005). In this study, we have been selected based on the average stress and their gradients in the vicinity of singular point. The gradient effect is taken into account by the first order derivative. The non-local stresses are then defined as:

$$\widetilde{\sigma}_{ij} = \begin{cases} \sigma_{ij} & \text{if } y = 0 \\ \sigma_{ij} + h \cdot \left(\dfrac{\partial \sigma_{ij}}{\partial x} + \dfrac{\partial \sigma_{ij}}{\partial y} + \dfrac{\partial \sigma_{ij}}{\partial z}\right) & \text{if } y > 0 \end{cases} \tag{5}$$

where h is characteristic length for taking into account the gradient effect. Note that h depends on the constituents, their geometries (lamina, woven-fabrics) of composites studied.

However, due to the main aim of this paper, we will investigate the delamination onset at interface of adjacent layers. As a result, we can suppose that the gradient effects have been only evaluated along the interface. The Eq. (5) can then be rewritten as:

$$\widetilde{\sigma}_{ij} = \begin{cases} \sigma_{ij} & \text{if } y = 0 \\ \sigma_{ij} + h \cdot \dfrac{\partial \sigma_{ij}}{\partial y} & \text{if } y > 0 \end{cases} \tag{6}$$

To summarize that, the average non-local stresses ($\overline{\widetilde{\sigma}}_{ij}$) which take into the effect of gradient on a neighborhood are determined upon the critical length.

The criterion that we proposed to prediction the delamination onset under fatigue loading is based on an extension of delamination onset criteria under quasi-static loading (Nimdum, 2009). Fatigue tests of woven-fabrics angle-ply laminates were performed in previous section. The interface of delamination onset and the number of cycles to delamination onset have been recorded. We assume that each ply remains undamaged until the onset of delamination and the interlaminar tensile and shear strength of the interface, which consist of three modes (I, II, III) and are determined by static tests, are damaged under fatigue loading. This degradation is related as a function of $\sigma_{\max}$, R, N and frequency (f). The delamination onset criterion under fatigue loading is then introduced as:

$$\left(\frac{\langle F_3 \rangle^{+}}{Y_T^{\text{Fatigue}}(N, \mathrm{f}, R, \sigma_{\max})}\right)^2 + \left(\frac{|F_1| + k_1 \langle F_3 \rangle^{-}}{S_1^{\text{Fatigue}}(N, \mathrm{f}, R, \sigma_{\max})}\right)^2 + \left(\frac{|F_2| + k_2 \langle F_3 \rangle^{-}}{S_2^{\text{Fatigue}}(N, \mathrm{f}, R, \sigma_{\max})}\right)^2 = 1 \tag{7}$$

In this study, R and f are constant at 0.1 and 1 Hz, respectively, to be able to simplify the equation above and to be rewritten as:

$$\left(\frac{\langle F_3\rangle^+}{Y_T \cdot f_1(N,\sigma_{\max})}\right)^2 + \left(\frac{|F_1| + k_1\langle F_3\rangle^-}{S_1 \cdot f_2(N,\sigma_{\max})}\right)^2 + \left(\frac{|F_2| + k_2\langle F_3\rangle^-}{S_2 \cdot f_3(N,\sigma_{\max})}\right)^2 = 1 \tag{8}$$

where Y_T^{Fatigue}, S_1^{Fatigue} and S_2^{Fatigue} represent the intralaminar tensile (mode I) and shear (mode II and III) strengths under cyclic loading, respectively, while Y_T S_1 and S_2 de II and III) are the intralaminar tensile (mode I) and shear (mode II and II) under quasi-static, respectively. $f_1(N,\sigma_{\max})$, $f_2(N,\sigma_{\max})$ and $f_3(N,\sigma_{\max})$ are the degradation function of interlaminar strengths as mode I, II and III, respectively. Assume that three modes are the same rate of degradation. In the same way as for static loading, two modes of interlaminar shear strength were assumed to be identical $(S_1 = S_2)$. The Eq. (8) can then be rewritten as:

$$\left(\frac{\langle F_3\rangle^+}{Y_T}\right)^2 + \left(\frac{|F_1| + k_1\langle F_3\rangle^-}{S}\right)^2 + \left(\frac{|F_2| + k_2\langle F_3\rangle^-}{S}\right)^2 = \left(f(N,\sigma_{\max})\right)^2 \tag{9}$$

In order to determine the degradation function, woven angle-ply laminate chosen are represented the predominant shear mode (III) to allow to neglect both mode I and mode II. Consequently, the criteria in the Eq. (9) can be simplified as:

$$\left(\frac{|\sigma_{13}|}{S}\right)_{\text{Non local}} = f(N,\sigma_{\max}) \tag{10}$$

where σ_{13} is the nonlocal stress, $\bar{\sigma}_{13}$ and $\tilde{\bar{\sigma}}_{13}$, at interface of delamination onset while S is the static interlaminar shear strength which are determined by non local method. Due to undamaged and in-plane isotropic behavior assumption until the delamination onset, it is useful to be able to determine the relation in Eq. (10) by the experimental results (macroscopic stress), (Figure 13). The degradation function of interlaminar strength under fatigue loading is given as:

$$\left(\frac{|\sigma|}{S}\right)_{\text{Non local}} = \left(\frac{\sigma_{\max}}{\sigma_{\text{onset}}}\right)_{\text{Macroscopic}} = f(N) = 1{,}032^{-(N-1)^{\frac{1}{3}}} \tag{11}$$

By substituting Eq. (11) into Eq. (9), we obtain the criterion for free-edge specimens as:

$$\left(\frac{\langle F_3\rangle^+}{Y_T}\right)^2+\left(\frac{|F_1|+k_1\langle F_3\rangle^-}{S}\right)^2+\left(\frac{|F_2|+k_2\langle F_3\rangle^-}{S}\right)^2=\left(1{,}032^{-(N-1)^{\frac{1}{3}}}\right)^2 \qquad (12)$$

In order to apply this criterion in Eq. (10) to circular-hole specimens, the interlaminar tensile and shear strengths in static case are modified. The transformation of coordinates as a function of angle of θ is used. θ is defined as illustrated in Figure 19. The delamination onset criterion during fatigue loading applied to circular-hole specimens is therefore shown in Eq. (13).

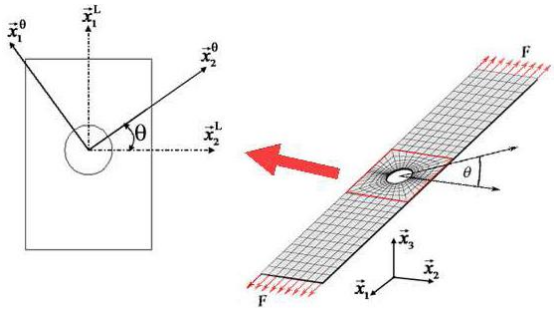

Figure 19. Configuration of circular-hole specimens

$$\begin{aligned}&\frac{\left(\langle F_3\rangle^+\right)^2}{Y_T^2}+\frac{\left(\langle F_3\rangle^-\right)^2}{S^2/(2k^2)}+\frac{|F_2|\langle F_3\rangle^-(\cos\theta+\sin\theta)}{S^2/(2k)}\\&+\frac{|F_1|\langle F_3\rangle^-(\cos\theta-\sin\theta)}{S^2/(2k)}+\frac{(F_2)^2}{S^2}+\frac{(F_1)^2}{S^2}=\left(1{,}032^{-(N-1)^{\frac{1}{3}}}\right)^2\end{aligned} \qquad (13)$$

5. Prediction of delamination onset in circular-hole specimens

This section an overview of the experimental tests and numerical simulations in circular-hole specimens is in order to validate the delamination onset criterion which was identified in previous section under cyclic loading

5.1. Experimental procedure

The specimen geometry for the open hole fatigue test had a hole diameter (ϕ) of 10 mm, a length (L) of 270 mm and a width (l) of 30 mm. The maximum applied stress at $\sigma_{\max}=0.6\sigma_R$ for $(0°,\pm20)_s$ and $(0°,\pm30)_s$, at $\sigma_{\max}=0.65\sigma_R$ for $(0°,\pm30_2)_s$ and at $\sigma_{\max}=0.7\sigma_R$ for $(0°,\pm20_2)_s$ were performed. The circular hole specimens

polished prior to testing are observed at different number of cycles level i.e. 100, 500, 1000, 5000, 1000, … etc. with the mirror which allow its to rotate around the axe (Figure 20a, 20b). The angle observation (α) is defined in Figure 20c. The $\alpha = 0°$ is parallel to the applied load direction.

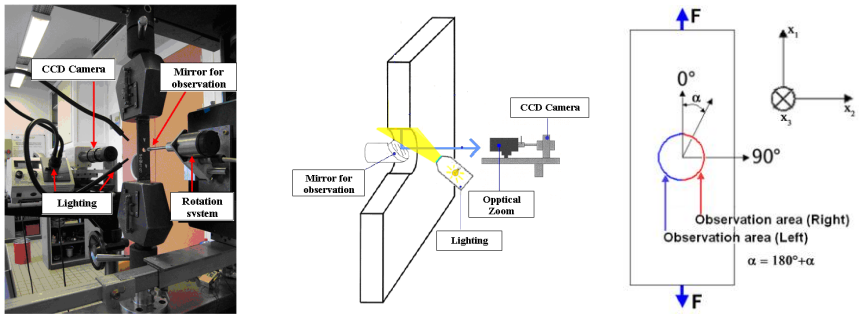

(a) (b) (c)

Figure 20. (a) Experimental setup; (b) Scheme of observation method; (c) Observation zone defined

5.2. Damage mechanism

The experimental observations of fatigue tests show that all specimens, whether the different thickness layers and stacking sequences, consist of three major damage (Figure 21): intra-ply cracking ("*a*"), the intra-ply delamination ("*b*") and finally inter-ply delamination ("*c*" and "*d*"). The effect of stacking sequence and thickness layer on the typical damages can then be neglected. Several intra-ply cracks firstly occur in the surface yarns. Then, the interlaminar delaminations occur in both interfaces, and finally their developed will joined with the intralaminar delamination which generally occur to follow along the curved yarns in ply (lamina).

It should be underline that typical damage mode of delaminage at the interfaces $+20°/-20°$ and $+30°/-30°$ is more difficult to observe due to interlaminar shear mode (mode III) representing the crack edges sliding without open mode. Consequently, the number of cycles to delamination onset determined in experimental testing remains uncertain. Thickness effect is no significant for delaminate onset location and the number of cycles to delamination onset, as shown in Table 5. On the other hand, we have found to affect significantly on the number of cycles to delamination onset with increasing the maximum stress level.

While, the interfaces $0°/+20°$ and $0°/+30°$, the delamination occur as a mixed mode representing not only crack edge sliding but also crack edge opening. The open mode is generally easier to observe because delaminations propagation, after their initiation, are spontaneous and rapid to allow clearly visualize.

Table 5. Experimental results during fatigue loading

Stacking sequence	Interfaces	Position of delamination onset ($\alpha°$)	Number of cycles to delamination onset (N_d)
$(0,\pm 20)_s$	$0/+20$	92 à 125	2000 – 3000
	± 20	83 à 97	260 - 700
$(0,\pm 20_2)_s$	$0/+20_2$	98 - 120	1660 - 3050
	$\pm 20_2$	84 - 100	125 - 450
$(0,\pm 30)_s$	$0/+30$	94 - 121	340 – 800
	± 30	82 - 100	215 – 600
$(0,\pm 30_2)_s$	$0_2/+30_2$	85 - 127	587 - 1250
	$\pm 30_2$	85 -95	50 – 220

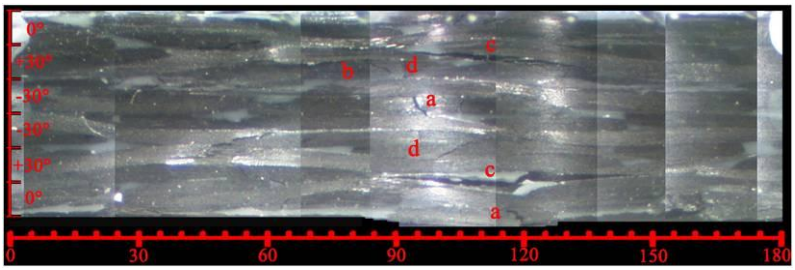

(a)

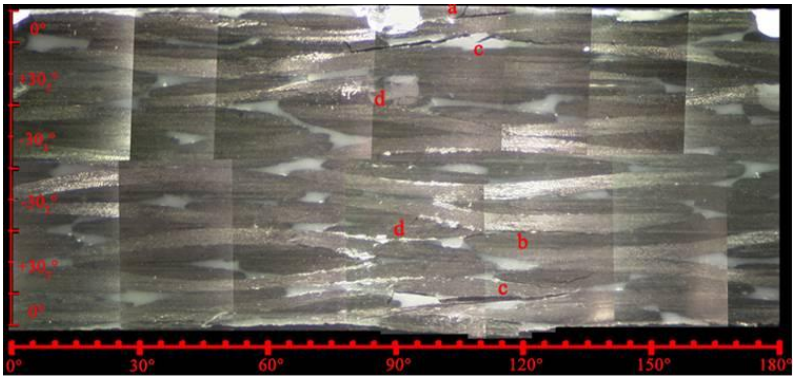

(b)

Figure 21. Damages mechanisms of fatigue loading for different stacking sequences: (a) $(0°,\pm 30°)_s$ *at 3000 cycles and (b)* $(0°,\pm 30°_2)_s$ *at 2000 cycles*

5.3. Delamination onset prediction: location and number of cycles

In order to carry out an in-depth understanding of damage mechanisms at edge of circular hole, the finite element method has been use. A uniform tensile stress, also called the macroscopic stress simulated, was applied along the direction of x_1-axis (longitudinal axis) of circular test specimen. All specimens show that the same regions of stress/strain distributions are illustrated. Figure 22, in case of $(0°,\pm 20°)_s$ laminate, shows high concentrations of σ_{11} and ε_{11} can be observed at $\alpha = \pm 90°$ around free-edge and nearly circular area (Figure 22a). Then we can also observe the strong stress singularities of σ_{33}, σ_{23} and σ_{13} at the interface between adjacent layers as shown in Figure 22b, c and d, respectively. These stresses relate directly to the delamination onset as explained in previous section.

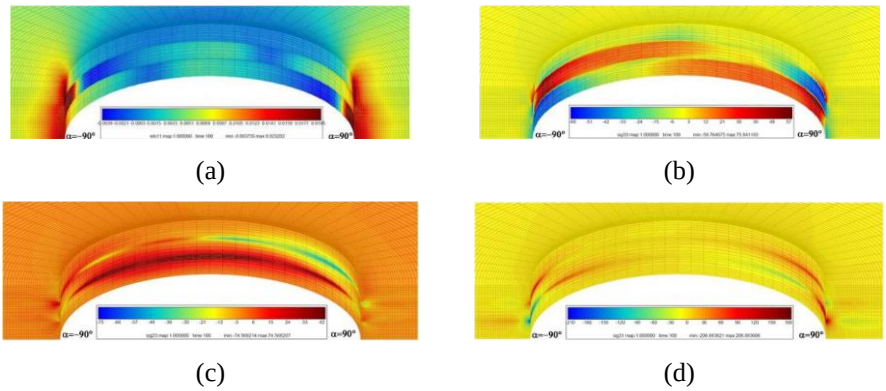

Figure 22. Distributions of stress-strain for $(0°,\pm 20°)_s$ *laminates around a free-edge and nearly circular hole area* $(-90° \le \alpha \ge 90°)$ $(0°,\pm 20)_s$ *: (a)* ε_{11} *;(b)* σ_{33}, *(c)* σ_{23} *and (d)* σ_{13}

The numerical results of all stacking sequences of a laminate composite show the good accuracy of location predictions to delamination onset compared with the experimental results, as example illustrate in Figure 23 for $(0°,\pm 30°)_s$ laminate case. The two approaches criterion, with and without gradients, predict to the same location of delamination onset. The numerical results show also a good correlation in term of damage mode (I, II and III) with experimental results.

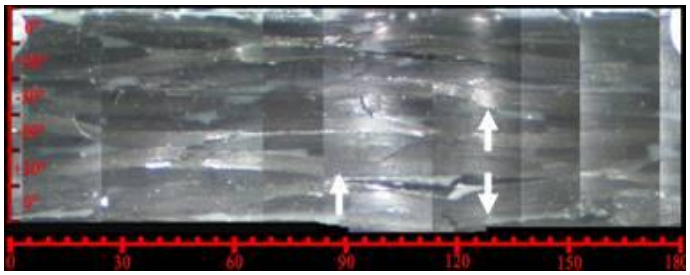

(a)

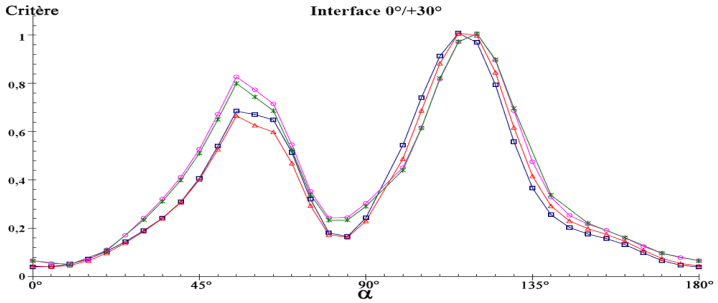

(b)

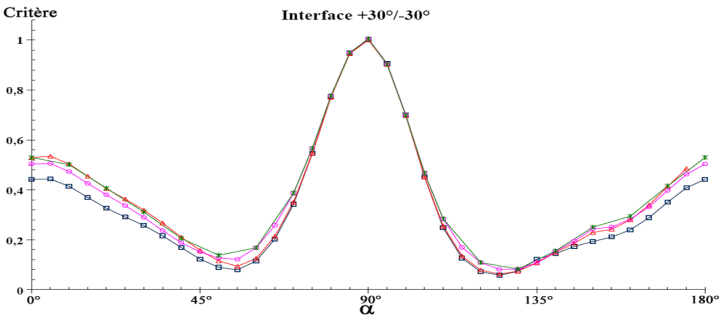

(c)

Figure 23. Delamination onset in $(0°,\pm 30°)_s$ *laminate around a free-edge circular hole: (a) experimental observed; (b) and (c) numerical prediction at interface* $0°/30°$ *and* $+30°/-30°$*, respectively*

For the prediction of number of cycles to delamination onset, there is a good correlation between the numerical results and experimental observations. The close predictions obtained for $0°/20°$ and $0°/30°$ interfaces while the slight prediction error of $+20°/-20°$ and $+30°/-30°$ interfaces can be found (Table 6). We suppose that the slight prediction error is caused by a typical mode III-type of delamination onset which is dominant in these interfaces. Consequently, this mode of

delamination onset is more difficult to observe due to the closing mode. To overcome this problem, high accuracy observation techniques like acoustic emission are necessary.

Table 6. Numerical result for prediction of delamination onset under fatigue loading

Stacking sequence	Interfaces	Numerical results of number of cycle to delamination onset			
		h = 0,0	h = 0,01	h = 0,02	h = 0,03
$(0,\pm 20)_s$	$0/+20$	3280	3800	10800	11500
	$+20/-20$	150	600	2100	2900
$(0,\pm 20_2)_s$	$0/+20_2$	3200	3700	9010	9600
	$+20_2/-20_2$	0	18	350	560
$(0,\pm 30)_s$	$0/+30$	250	450	2000	2400
	$+30/-30$	17	135	375	650
$(0,\pm 30_2)_s$	$0_2/+30_2$	370	600	1950	2350
	$+30_2/-30_2$	0	0	2	15

6. Conclusions

An experimental investigation and FEM in two families, unidirectional and angle-ply 2/2 twill weave T800 carbon/epoxy woven fabric composites laminates, under fatigue loading have been presented in this paper. This study can be summarized as follow:

1) Unidirectional woven fabric composite laminates:

– Effect of thickness ($n > 4$) for variation of rigidities, the thresholds of damage in 0°-ply laminate is neglect;

– Increasing the maximum applied stress accelerates the stiffness reduction and the damage evolution;

– The cracking in warp yarn and the intralaminar delamination are the major damage;

– The numerical simulation with FEM was used to investigate the woven effects on the out-of-phase case and show that the local bending provokes the local stress (or strain) concentrates which have a good correlation with the damage zone in experimental observation;

– The homogenization methods applied to the damaged material show that the stiffness reduction of 20% is caused by the delamination. This result is a good agreement with experimental testing.

2) Angle-ply woven fabric composite laminates:

– Due to the high interlaminar normal and interlaminar shear stress gradients at the free-edge region, the inter-ply delamination represent as the main damage to allow the stiffness reduction and final break. Increasing of number of plies (thickness effect) does not affect to the damage mechanism;

– The fatigue non-local criteria model (with and without gradient), which are identified the parameters by experimental Edge Delamination Tests (EDT), have been proposed to predict the delamination onset and to overcome the mesh-dependence problems;

– Validation criteria was applied on the circular-hole specimens and shown a good prediction the position of delamination onset. For the prediction of number of cycles to delamination onset, the close predictions obtained for $0°/20°$ and $0°/30°$ interfaces while the slight prediction error of $+20°/-20°$ and $+30°/-30°$ interfaces can be found due to precision error which occurs from the difficult observation of delamination onset in shear mode.

We propose high accuracy observation techniques like the acoustic emission which allow more accurate monitoring and early detection of decohesion or slipping in shear mode within the material. Emission acoustic technique has many advantages such as in situ monitoring without removing the specimen and accuracy of damage detection. But the difficulty is to correlate between the acoustic signals and the typical damages.

Acknowledgements

We gratefully acknowledge ADEME (Agence de l'Environnement et de la Maîtrise de l'Energie) for support from ARMINES Centre des Matériaux, in the project LICOS and ALSTOM.

References

Alif N., Carlsson L.A., et Boogh L. (1998). The effect of weave pattern and crack propagation direction on mode I delamination resistance of woven glass and carbon composites, *Composites:Part B*, vol. 29B, p. 603-611.

Bažant Z.P. et Pijaudier-Cabot G. (1998). Nonlocal continuum damage, localization instability and convergence, *Journal of Applied Mechanics*, vol. 55, p. 287-293.

Bond I.P. (1999). Fatigue life prediction for GRP subjected to variable amplitude loading, *Composites: Part A*, vol. 30, p. 961-970.

Brewer J.C. et Lagace P.A. (1988). Quadratic Stress Criterion for Initiation of delamination, *Journal of Composite Materials*, vol. 22, p. 1141-1155.

Broutman L.J. et Sahu S. (1972). A new theory to predict cumulative fatigue damage in fiber glass reinforced plastics *Composite materials: testing and design*, (2nd conference). ASTM STP, 497, p. 170-188.

Caron J.-F. (1993). *Modélisation de la cinétique de fissuration transverse en fatigue dans les stratifiés*, PhD thèse,Ecole Nationale des Ponts et Chaussées.

Demers C.E. (1998). Tension-tension axial fatigue of E-glasse fibre-reinforced polymeric composites : fatigue life diagram, *Construction and Building Materials*, vol. 12, p. 303-310.

Fawaz Z et Ellyin F. (1994). Fatigue failure model for fibre-reinforced materials under general loading conditions, *Journal of Composite Materials*, vol. 28(15), p. 1432-1451.

Germain N., Besson J., Feyel F. et Maire J.F. (2005). Méthodes de calcul non local appliquées au calcul de structures composites, *Compiègne JNC14*, vol. 2, p. 633-640.

Hashin, Z. et Rotem, A. (1973). A fatigue criterion for fibre reinforced composite materials, *Journal of Composite Material*, vol. 7, p.448-464.

Joo J.W. (1992). A failure Criterion for laminates governed by free edge interlaminar shear stress, *Journal of Composite Materials*, vol. 26(10), p. 1510-1522.

Kelkar A.D., Tate J.S. et Bolick R. (2006). Structural integrity of aerospace textile composites under fatigue loading, *Material Science and Engineering B*, vol. 132, p. 79-84.

Kim R.Y., and Soni S.R. (1984). Experimental and Analytical Studies on the onset of delamination in laminated composites, *Journal of Composites Materials*, vol. 18, p. 71-80.

Lorriot Th., Marion G., Harry H., et Wargnier H. (2003). Onset of free-edge delamination in composite laminates under tensile loading, *Composites:Part B*, vol. 34, p. 459-471.

Nicoletto G. et Riva E. (2004). Failure mechanisms in twill-weave laminates: FEM predictions vs. experiment, *Composites: Part A*, vol. 35, p. 787-795.

Nimdum P. (2009). *Dimensionnement en fatigue des structure ferroviaire en composites épais*, PhD thèse, Ecole des Mines de Paris.

Pandita S. D., Huvsmans G., Wevers M., et Verpoest I. (2001). Tensile fatigue behaviour of glass plain-weave fabric composites in on- and off-axis directions, *Composites: Part A*, vol. 32, p. 1533-1539.

Philippidis T.P. et Vassilopoulos A.P. (1999). Fatigue of composite laminates under off-axis loading, *International Journal of Fatigue*, vol. 21, p. 253-262.

Talreja R. (2003). Fatigue of polymer matrix composites. *Comprehensive Composite Materials*, Chapter 2.14, p. 529-552.

Thionnet A. et Renard J. (1994). Laminated composites under fatigue loading : a dammage development law for transverse cracking, *Composite Science Technology*, vol. 52, p. 173-181.

Thionnet A. et Renard J. (1997). Modelling of the fatigue behaviour of laminated composite structures, In : Degallaix, S., Bathias, C. et Fougères, R. (eds.). *International Conference on fatigue of composites*. Proceedings, 3-5 June, Paris, Frace. La Société Française de Métallurgie et de Matériaux, pp. 363-369.